Acta Crystallographica Section A
Foundations of Crystallography
ISSN 0108-7673

Received 26 April 2012
Accepted 13 July 2012

Experimental determination of spin-dependent electron density by joint refinement of X-ray and polarized neutron diffraction data

Maxime Deutsch,[a,b] Nicolas Claiser,[a,b] Sébastien Pillet,[a,b] Yurii Chumakov,[a,c,d] Pierre Becker,[c] Jean-Michel Gillet,[c] Béatrice Gillon,[d] Claude Lecomte[a,b] and Mohamed Souhassou[a,b]*

[a]Université de Lorraine Laboratoire de Cristallographie, Résonance Magnétique et Modélisations, UMR 7036 Vandoeuvre-lès-Nancy, F-54506 France, [b]CNRS Laboratoire de Cristallographie, Résonance Magnétique et Modélisations, UMR 7036 Vandoeuvre-lès-Nancy, F-54506 France, [c]Laboratoire SPMS, UMR CNRS 8580, École Centrale Paris, Grande Voie des Vignes, 92295 Chatenay-Malabry, France, and [d]Laboratoire Léon Brillouin (CEA-CNRS, UMR 12), Centre d'Etudes de Saclay, 91191 Gif-sur-Yvette, France. Correspondence e-mail: mohamed.souhassou@crm2.uhp-nancy.fr

New crystallographic tools were developed to access a more precise description of the spin-dependent electron density of magnetic crystals. The method combines experimental information coming from high-resolution X-ray diffraction (XRD) and polarized neutron diffraction (PND) in a unified model. A new algorithm that allows for a simultaneous refinement of the charge- and spin-density parameters against XRD and PND data is described. The resulting software *MOLLYNX* is based on the well known Hansen–Coppens multipolar model, and makes it possible to differentiate the electron spins. This algorithm is validated and demonstrated with a molecular crystal formed by a bimetallic chain, $MnCu(pba)(H_2O)_3{\cdot}2H_2O$, for which XRD and PND data are available. The joint refinement provides a more detailed description of the spin density than the refinement from PND data alone.

1. Introduction

Electron density, in all its representations, plays a key role in the understanding of the nature of chemical bonds. The tremendous improvement of X-ray sources, detectors and software has significantly increased the resolution and the quality of diffraction data, allowing a precise determination of the atomic electron distribution when a multipolar model is used (Stewart, 1976; Hirshfeld, 1977; Hansen & Coppens, 1978).

According to the Hohenberg–Kohn theorem (Hohenberg & Kohn, 1964), if such an approach was to yield an exact experimental electron density, every other piece of information for the system (at least in the ground state) would be within reach. However, to this day, and despite the efforts of a large community of crystallographers, experimental charge-density modelling has not reached this stage. Additional information can be obtained in the case of magnetic materials by polarized neutron diffraction. This technique has proved to be a valuable tool for determining the electronic spin distribution. In addition, inelastic X-ray scattering (in the high momentum and energy transfer regime) turns out to be highly sensitive to the most delocalized electrons. Therefore, this spectroscopy should be considered as very complementary to the previously cited coherent elastic scattering techniques.

From the X-ray and neutron scattering standpoint, the one-particle reduced-density matrix (1-RDM) can be seen as a unifying quantity (Gillet, 2007). The definition of the 1-RDM derives from the N particles wavefunction $\psi(\mathbf{x}_1, \mathbf{x}_2, \ldots, \mathbf{x}_N)$, where $\mathbf{x}_j$ stands for both the position $\mathbf{r}_j$ and the spin coordinate of particle j,

$$\Gamma_1(\mathbf{x}_1\,\mathbf{x}'_1) = N \int \psi^*(\mathbf{x}_1, \mathbf{x}_2, \ldots, \mathbf{x}_N)\psi(\mathbf{x}'_1, \mathbf{x}_2, \ldots, \mathbf{x}_N)\,\mathrm{d}^4x_2 \ldots \mathrm{d}^4x_N$$

for a pure state.

The charge $\rho_\uparrow(\mathbf{r}) + \rho_\downarrow(\mathbf{r})$ and spin $\rho_\uparrow(\mathbf{r}) - \rho_\downarrow(\mathbf{r})$ densities are related to the 'diagonal part of the 1-RDM'; they are obtained by merely integrating over all the spin variables and setting $\mathbf{r}'_1 = \mathbf{r}_1 = \mathbf{r}$:

$$\int\left[\delta(s - s_\uparrow) \pm \delta(s - s_\downarrow)\right]\Gamma_1(\mathbf{x}; \mathbf{x}')_{\mathbf{x}=\mathbf{x}'}\,\mathrm{d}s = \rho_\uparrow(\mathbf{r}) \pm \rho_\downarrow(\mathbf{r}).$$

The diagonal part of the 1-RDM can thus be recovered from X-ray and polarized neutron diffraction.

Several papers report on the possibility of recovering the full 1-RDM from X-ray diffraction data only either by jointly minimizing the resulting energy (Jayatilaka & Grimwood,

2001) or imposing mathematical constraints such as idempotency (Massa *et al.*, 1985; Howard *et al.*, 1994). It is noteworthy that attempts to combine X-ray and polarized neutron data were first proposed by Becker & Coppens (1985), followed by other members of Coppens' group (Coppens *et al.*, 1986, 1999; Koritsanszky & Coppens, 1986) without significant success.

This paper is dedicated to the simultaneous determination of the charge and spin densities in a unified refinement strategy. Until now they have instead been determined separately, and interpreted conjointly (Williams *et al.*, 1981; Figgis *et al.*, 1989; Claiser *et al.*, 2005). We therefore describe in this paper how to build a phenomenological model gathering data originating from different diffraction experiments such as X-ray (XRD), unpolarized neutron (UND) and polarized neutron (PND) diffraction. This paper is mostly oriented towards methodological aspects:

(*a*) How to combine different sets of data?

(*b*) How to build a common model adapted to a joint refinement?

(*c*) How to fruitfully exploit this new model?

This proposed method is then validated and demonstrated with a molecular bimetallic chain system, composed of Mn^{II} and Cu^{II} ions antiferromagnetically coupled through an oxamato bridge (Baron *et al.*, 1997; Pillet *et al.*, 2004).

The implementation of the joint refinement algorithm in the new software *MOLLYNX* and the appropriate refinement strategy are presented in §2. The application of the joint refinement procedure to the consecutive determination of the charge density, spin density and spin-dependent charge densities is discussed in detail in §3.

2. Methodology for modelling charge and spin densities

Charge- and spin-density distributions can be obtained separately from XRD and PND data, respectively, using the Hansen & Coppens multipolar model (Hansen & Coppens, 1978) in which the atomic charge density is given by

$$\rho(\mathbf{r}) = \rho_{\rm core}(r) + P_{\rm v}\kappa^3\rho_{\rm v}(\kappa r) + \sum_{l=0}^{l_{\rm max}} \kappa'^3 R_l(\kappa' r) \sum_{m=0}^{l} P_{lm\pm} y_{lm\pm}(\theta, \varphi), \quad (1)$$

where $\rho_{\rm core}$ and $\rho_{\rm v}$ are the core and valence spherical contributions to the charge density. The deformation charge density is developed on real spherical harmonic functions $y_{lm\pm}(\theta, \varphi)$, with radial extension $R_l(\kappa r)$ usually of Slater type. $P_{\rm v}$ and $P_{lm\pm}$ are the valence and multipolar population parameters, respectively. κ and κ' are the contraction/expansion parameters. The refined parameters of the model are $P_{\rm v}$, $P_{lm\pm}$, κ and κ'. The spin density is modelled in a similar manner, as described by Brown *et al.* (1979), Ressouche *et al.* (1993) and Zheludev *et al.* (1994):

$$s(\mathbf{r}) = P^{\rm s}_{\rm v}\kappa^3\rho_{\rm v}(\kappa r) + \sum_{l=0}^{l_{\rm max}} \kappa'^3 R_l(\kappa' r) \sum_{m=0}^{l} P^{\rm s}_{lm\pm} y_{lm\pm}(\theta, \varphi), \quad (2)$$

where $P^{\rm s}_{\rm v}$ is the population of the valence electrons with unpaired spin, and $P^{\rm s}_{lm\pm}$, κ and κ' are the refined spin-density parameters. The assumption has been made that there is no core contribution to the spin density.

As the charge and spin densities are described by a similar multipolar atom-centred model with a common parameterization, it makes a combined treatment of the two quantities possible. For this purpose, the valence populations ($P_{\rm v}$), multipolar populations ($P_{lm\pm}$) and expansion/contraction parameters (κ, κ') may be split for magnetic atoms (atoms carrying a spin magnetic moment) into two components with respect to the spin (up or down). The charge density (respectively, spin density) is simply the sum (respectively, difference) of the up-spin and down-spin electron densities as given in equation (3) [respectively, (4)].

$$\begin{aligned}\rho(\mathbf{r}) &= \rho^{\uparrow}(\mathbf{r}) + \rho^{\downarrow}(\mathbf{r}) \\ &= \rho_{\rm core}(r) + P^{\uparrow}_{\rm v}\kappa^{\uparrow 3}\rho^{\uparrow}_{\rm v}(\kappa^{\uparrow} r) + P^{\downarrow}_{\rm v}\kappa^{\downarrow 3}\rho^{\downarrow}_{\rm v}(\kappa^{\downarrow} r) \\ &\quad + \sum_{l=0}^{l_{\rm max}} \kappa'^{\uparrow 3} R_l(\kappa'^{\uparrow} r) \sum_{m=0}^{l} P^{\uparrow}_{lm\pm} y_{lm\pm}(\theta, \varphi) \\ &\quad + \sum_{l=0}^{l_{\rm max}} \kappa'^{\downarrow 3} R_l(\kappa'^{\downarrow} r) \sum_{m=0}^{l} P^{\downarrow}_{lm\pm} y_{lm\pm}(\theta, \varphi), \end{aligned} \quad (3)$$

$$\begin{aligned} s(\mathbf{r}) &= \rho^{\uparrow}(\mathbf{r}) - \rho^{\downarrow}(\mathbf{r}) \\ &= P^{\uparrow}_{\rm v}\kappa^{\uparrow 3}\rho^{\uparrow}_{\rm v}(\kappa^{\uparrow} r) - P^{\downarrow}_{\rm v}\kappa^{\downarrow 3}\rho^{\downarrow}_{\rm v}(\kappa^{\downarrow} r) \\ &\quad + \sum_{l=0}^{l_{\rm max}} \kappa'^{\uparrow 3} R_l(\kappa'^{\uparrow} r) \sum_{m=0}^{l} P^{\uparrow}_{lm\pm} y_{lm\pm}(\theta, \varphi) \\ &\quad - \sum_{l=0}^{l_{\rm max}} \kappa'^{\downarrow 3} R_l(\kappa'^{\downarrow} r) \sum_{m=0}^{l} P^{\downarrow}_{lm\pm} y_{lm\pm}(\theta, \varphi). \end{aligned} \quad (4)$$

$P^{\uparrow}_{\rm v}$ and $P^{\downarrow}_{\rm v}$ are the spin-dependent valence populations, while $P^{\uparrow}_{lm\pm}$ and $P^{\downarrow}_{lm\pm}$ are the spin-dependent multipolar populations. The sum of the spin-dependent valence populations is equal to the valence population $P_{\rm v}$ in equation (1), while the difference corresponds to the spin valence population $P^{\rm s}_{\rm v}$ in equation (2). Non-magnetic atoms are simply described by equation (1). In the most general case, the spin-up and spin-down distributions may not have identical radial extension. This can be taken into account by defining different spin-dependent contraction–expansion parameters $\kappa^{\uparrow}/\kappa^{\downarrow}$ and $\kappa'^{\uparrow}/\kappa'^{\downarrow}$.

In order to combine these data, the following assumptions have been made:

(*a*) The cell parameters used are those obtained from the single-crystal X-ray experiments, since they are usually better estimated from X-ray than from neutron experiments.

(*b*) Two sets of thermal displacement parameters are refined, one for the X-ray data and one for the neutron data, due to the possible difference between static and dynamic disorder [small (X-ray) and large (neutron) crystals].

(*c*) Constraints on electroneutrality and total magnetic moment are implemented using the Hamilton method (Hamilton, 1965).

In this joint refinement strategy, the sum of the spin valence populations over the atoms of the molecular unit is constrained to be equal to the number of unpaired electrons corresponding to the total spin state of the molecular unit, estimated from chemical grounds. Therefore, the scale factor

refined for PND in this work provides a value of the net magnetization of the single-crystal sample under the conditions of magnetic field and temperature during the PND data collection. It may be directly compared with magnetization measurements [superconducting quantum interference device (SQUID) measurements] under the same conditions of magnetic field and temperature.

The joint refinement algorithm implemented in the new software *MOLLYNX* is based on the usual least-squares procedure, for which the minimized function χ^2 is defined as

$$\chi^2(p) = \sum_{\mathbf{H}} \left|F^{\rm O}_{\mathbf{H}} - F^{\rm C}_{\mathbf{H}}(p)\right|^2 / \sigma^2(F^{\rm O}_{\mathbf{H}}),$$

where p stands for all parameters of the model (scale factors, atomic positions x, y, z, atomic displacement parameters $U_{ij}{}^{\rm X}$, $U_{ij}{}^{\rm N}$, multipolar population P_{lm} ...), $\mathbf{H}$ runs over all the measured/calculated structure-factor amplitudes $F^{\rm O}/F^{\rm C}$, σ being the estimated standard deviation of $F^{\rm O}$, and

$$F^{\rm C}(\mathbf{H}) = \sum_j f_j(\mathbf{H}) \exp(2i\pi \mathbf{H}\cdot\mathbf{r}) T_j(\mathbf{H}),$$

where $T_j(\mathbf{H})$ is the Debye–Waller factor,

$$\begin{aligned} f_j(\mathbf{H}) = {} & \frac{1\pm 1}{2} f_{\rm core}(\mathbf{H}) + P_{\rm v}^{\uparrow} f_{\rm v}(H/\kappa^{\uparrow}) \pm P_{\rm v}^{\downarrow} f_{\rm v}(H/\kappa^{\downarrow}) \\ & + \sum_{l=0}^{l_{\max}} \Phi_l(H/\kappa'^{\uparrow}) \sum_{m=0}^{l} P^{\uparrow}_{lm\pm} y_{lm\pm}(\mathbf{H}/H) \\ & \pm \sum_{l=0}^{l_{\max}} \Phi_l(H/\kappa'^{\downarrow}) \sum_{m=0}^{l} P^{\downarrow}_{lm\pm} y_{lm\pm}(\mathbf{H}/H), \end{aligned}$$

where + and − hold for XRD and PND, respectively. When dealing with different data sets for one common model, the question of the weighting scheme naturally arises. It then becomes essential to construct a function to minimize, possibly based on individual χ^2, assigning a fair weight to each data set. The section below describes the weighting schemes that have been considered for such a joint refinement.

2.1. Weighting schemes

One of the main concerns in the joint refinement strategy is the weighting scheme for the different data sets, because we deal with an almost complete high-resolution X-ray data set (~10 000 reflections for a maximal resolution of about 1 Å^{-1}) compared to a medium resolution and incomplete neutron data set (~1000 reflections for UND and a few hundreds for PND, with a maximal resolution of about 0.5 Å^{-1}). Three weighting schemes have been considered:

(i) The first scheme uses a score function C that minimizes the sum of the χ^2 values of each experiment. This weight usually favours the experiment that provides a large data set; such a model has been used, for example, in the joint refinement of H atoms in structural (Duckworth *et al.*, 1969) and charge-density studies (Coppens *et al.*, 1981), in the powder-diffraction community (Williams *et al.*, 1988) and for joint X-ray and neutron protein-structure refinements (Wlodawer & Hendrickson, 1982; Adams *et al.*, 2009). The minimized function is defined as

$$C\left(\left\{\chi_j^2(p)\right\}\right) = \sum_j \chi_j^2(p),$$

where j stands for an experiment (X-ray, neutron, ...) and p refers to the parameters of the model. The individual $\chi_j^2(p)$ function is defined as

$$\chi_j^2(p) = \sum_i \left|F_i^{j\,\rm O} - F_i^{j\,\rm C}(p)\right|^2 / \sigma^2(F_i^{j\,\rm O}),$$

where i runs over all the measured/calculated structure-factor amplitudes $F^{\rm O}/F^{\rm C}$ and σ is the estimated standard deviation associated with $F^{\rm O}$. The derivative of C is the sum of the gradients of individual $\chi_j{}^2$,

$$\vec{\nabla} C\left(\left\{\chi_j^2(p)\right\}\right) = \sum_j \vec{\nabla}\chi_j^2(p),$$

and the inverse of the covariance matrix is the sum of the individual inverse of the covariances:

$$\frac{\partial^2 C\left(\left\{\chi_j^2(p)\right\}\right)}{\partial p_l \partial p_k} = \sum_j \frac{\partial^2 \chi_j^2(p)}{\partial p_l \partial p_k}.$$

This weighting scheme is called hereafter UNIT.

(ii) The second weighting scheme, called 'total ignorance weighting scheme', was proposed by Bell *et al.* (1996) and Gillet *et al.* (Gillet *et al.*, 2001; Gillet & Becker, 2004; Gillet, 2007); it is based on the logarithm of χ^2, which reduces the weighting ratio between large and small data sets and hence should better take into account the contribution of the small data set (at least at the beginning of the refinement procedure). Another reason for using this weighting scheme originates from the large variation of standard-deviation estimates from one data-reduction method (software dependent) to another. The 'total ignorance' scheme is built upon the assumption that there exists an overall scaling uncertainty on each standard-deviation set:

$$C\left(\left\{\chi_j^2(p)\right\}\right) = \sum_j N_j \log(\chi_j^2(p)),$$

where N_j stands for the number of measured data in the jth experiment,

$$\begin{aligned} & \vec{\nabla} C\left(\left\{\chi_j^2(p)\right\}\right) = \sum_j N_j \frac{\vec{\nabla}\chi_j^2(p)}{\chi_j^2(p)}, \\ & \frac{\partial^2 C\left(\left\{\chi_j^2(p)\right\}\right)}{\partial p_l \partial p_k} \\ & \quad = \sum_j N_j \left[\frac{\partial^2 \chi_j^2(p)}{\partial p_l \partial p_k}\frac{1}{\chi_j^2(p)} - \frac{\partial \chi_j^2(p)}{\partial p_l}\frac{\partial \chi_j^2(p)}{\partial p_k}\left(\frac{1}{\chi_j^2(p)}\right)^2\right]. \end{aligned}$$

Hereafter, this weighting scheme will be referred to as NLOG. In this model the logarithm function is scaled by the size of the data set (N) and it also leads to a weight ratio equivalent to the sample sizes ratio, which slightly favours the large data set.

(iii) We therefore decided to introduce a third weighting scheme based only on the sum of logarithms. The score function and its derivatives are

Table 1
Refined parameters for each type of data set.

Sc is the scale factor, U^{ij} are the anisotropic atomic displacement parameters. * indicates the data set used if the cos(α) constraint is applied (see text).

Data set	Sc_X	Sc_N	Sc_{PN}	κ, κ'	x, y, z	U^{ijX}	U^{ijN}	$P_v^{\uparrow}+P_v^{\downarrow}$, $P_{lm}^{\uparrow}+P_{lm}^{\downarrow}$	$P_v^{\uparrow}-P_v^{\downarrow}$, $P_{lm}^{\uparrow}-P_{lm}^{\downarrow}$
XRD	×			×	×	×		×	×*
UND		×			×		×		
PND			×	×				×*	×

$$C\left(\left\{\chi_j^2(p)\right\}\right)=\sum_j \log(\chi_j^2(p)),\quad \vec{\nabla}C(\chi_j^2(p))=\sum_j \frac{\vec{\nabla}\chi_j^2(p)}{\chi_j^2(p)}$$

$$\frac{\partial^2 C\left(\left\{\chi_j^2(p)\right\}\right)}{\partial p_l \partial p_k}=\sum_j \frac{\partial^2\chi_j^2(p)}{\partial p_l \partial p_k}\frac{1}{\chi_j^2(p)}-\frac{\partial\chi_j^2(p)}{\partial p_l}\frac{\partial\chi_j^2(p)}{\partial p_k}\frac{1}{\left(\chi_j^2(p)\right)^2}.$$

This weighting scheme is hereafter called LOG.

In principle, the NLOG or LOG scheme may prevent the neglect of small data sets. It actually turns out that these different weighting schemes seem to lead to the same 'global minimum'. However, as they do not have the same 'local minima', a change of the weighting scheme during the refinement would be a possible way to escape from a false 'local minimum'.

For the test example (see below) the ratios between the XRD and PND weights at the end of the refinement were typically $w^X/w^{PN}\simeq 20$, $w^X/w^{PN}\simeq 44$ and $w^X/w^{PN}\simeq 1.4$ for the UNIT, NLOG and LOG weighting schemes, respectively. (The number of reflections are 6880 and 228 for XRD and PND, respectively.) However, it should be noted that these weighting ratios are only global indicators and that some parameters are essentially determined exclusively by one of the data sets [see Coppens *et al.* (1981) for the relative dependence of some joint parameters]. If no constraints are applied (see the next section), the spin parameters depend only on the PND data. The corresponding diagonal matrix elements therefore have no contribution from the other data sets and the 'mixed' off-diagonal terms are zero.

2.2. Refinement and constraints

This original refinement method has been implemented in the new software *MOLLYNX* derived from *MOLLY* (Hansen & Coppens, 1978). Table 1 shows the dependence of the refined parameters against the various data sets, *i.e.* atomic positions are refined against XRD and UND data, κ/κ' are determined by both XRD and PND data. The multipolar parameters $P_{lm\pm}^{\downarrow\uparrow}$ are common to both XRD and PND if there is a constraint between the charge- and spin-density parameters (see next section).

During the first tests of the refinement, large correlations were observed between spin-up and spin-down multipolar parameters. As a consequence, in some cases spin populations turned out to be larger than charge populations for a given multipole (*i.e.* more unpaired electrons than total electrons). As shown by Table 1, these correlations are a direct consequence of the joint refinement procedure during which the XRD data fix the charge-density parameters, whereas PND data are used to fit the spin population without any physical relationship between the two densities except the radial extension. Such a joint refinement must therefore be constrained in order to ensure that the charge density in a given multipole is always greater than the spin density. This can be formally expressed as

$$\left|P_{lm\pm}^{\uparrow}+P_{lm\pm}^{\downarrow}\right|\geq\left|P_{lm\pm}^{\uparrow}-P_{lm\pm}^{\downarrow}\right|.$$

A first brute-force possibility to enforce this constraint on the split multipoles is the following: if after one cycle of least-squares refinement up and down populations of a given multipole lead to a spin population larger than the charge one, then the spin population is set equal to the charge population to satisfy the previous relation. This constraint is an *a posteriori* constraint applied after each refinement cycle. This is unsatisfactory, since there remains a possibility that the next iteration will end up similarly.

A more efficient way to satisfy the previous inequality is to use a bounded function such as 'cos(α)':

$$P_{lm\pm}^{\uparrow}-P_{lm\pm}^{\downarrow}=\cos(\alpha)(P_{lm\pm}^{\uparrow}+P_{lm\pm}^{\downarrow}).$$

Then refining α and the charge-density multipoles ($P_{lm\pm}^{\uparrow}+P_{lm\pm}^{\downarrow}$) is equivalent to refining $P_{lm\pm}^{\uparrow}$ and $P_{lm\pm}^{\downarrow}$. The main disadvantage of this method is that it leads to a nonlinear least-squares refinement. To reduce this effect, we added the second derivatives with respect to α to the least-squares process. (See Appendix A for more computational details.)

3. Application, results and discussion

In order to test the joint refinement procedure, we chose as a prototype system the bimetallic chain compound $MnCu(pba)(H_2O)_3\cdot 2H_2O$, where pba is 1,3-propylene bis(oxamato) (Fig. 1), for which a detailed charge-density (at 114 K) and a spin-density (at 10 K) analysis have been reported by Pillet *et al.* (2004) and Baron *et al.* (1997) from XRD and PND measurements, respectively.

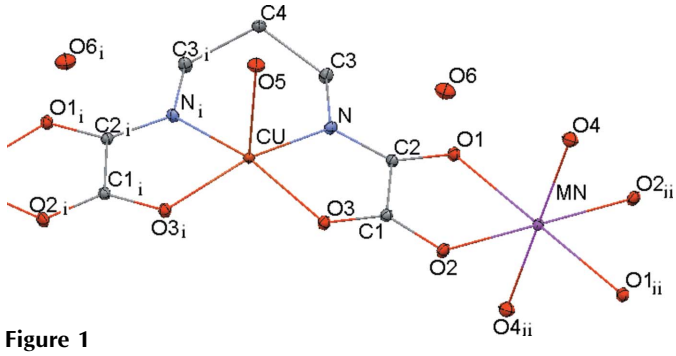

Figure 1
ORTEP representation of the Mn—Cu chain structure at 10 K; thermal displacement ellipsoids are plotted at the 50% probability level. Symmetry codes: (i) x, 1/2 − y, z, (ii) −x, −y, −z.

Table 2
XRD and PND experimental conditions.

Chemical formula: $MnCu(pba)(H_2O)_3{\cdot}2H_2O$ ($MnCuC_7N_2O_{11}H_{16}$). Space group: *Pnma*; cell parameters: $a = 12.7858$ (5), $b = 21.2972$ (8), $c = 5.1864$ (2) Å.

	Experiment	
	X-ray	Polarized neutron
No. of unique reflections	6880 [$I > 3\sigma(I)$]	228
Temperature (K)	10	10
Wavelength (Å)	0.71073	0.83
Maximum sin θ/λ (Å^{-1})	1.13	0.49

This molecular crystal is built from infinite oxamato-bridged Mn^{II}–Cu^{II} chains running along the crystallographic *b* axis in the orthorhombic space group *Pnma* (Fig. 2) (Pei *et al.*, 1987). The Mn atom lies on an inversion centre in an elongated octahedral coordination, while Cu, O5, C4, H1 and H2 lie on a mirror plane (H atoms are omitted in the figure). The water molecule (O4) is located in the elongated apical direction [Mn—O4 = 2.1894 (5) Å], whereas the axial positions are occupied by the O1 and O2 atoms of the oxamato bridge [Mn—O basal = 2.1645 (4) and 2.1812 (5) Å]. The Cu atom is located on a crystallographic mirror plane in a pyramidal environment coordinated by one water molecule (O5) in the apical direction and two atoms (O, N and symmetry equivalents) in the basal plane, 0.245 Å below the Cu position.

Neighbouring chains are connected in the *ac* plane by four short hydrogen bonds involving the O1 and O2 atoms and the lattice water molecule O6. The O···H distances range from 1.89 (2) to 2.22 (2) Å. This is a quasi-one-dimensional crystal structure which involves similar long distances between the magnetic centres within [Mn···Cu = 5.4325 (1) Å] and between the chains [Mn···Mn = 6.8642 (1) and Cu···Cu = 6.4415 (2) Å].

The Cu^{II} and Mn^{II} cations are coupled antiferromagnetically through the oxamato bridge by a superexchange mechanism (Fig. 2), leading to a magnetic behaviour typical for one-dimensional ferrimagnetic ordered chains with weak interchain couplings (Pei *et al.*, 1987).

Since the charge-density study had been carried out at a much higher temperature than the spin-density study, a new high-resolution XRD data set at 10 K was collected to match closely the PND experiment; 61 774 reflections were collected with Mo $K\alpha$ radiation using a Supernova diffractometer equipped with a Helijet cryogenic system.[1] The data were corrected for absorption ($T_{min} = 0.64$ and $T_{max} = 0.88$), yielding 8505 unique reflections ($R_{int} = 0.0341$) of which $N_X = 6880$ [$I > 3\sigma(I)$] were used for the joint refinement to a maximum resolution of $(\sin\theta/\lambda)_{max} = 1.13$ Å^{-1}. The number of reflections in the PND data set is $N_{PN} = 228$ up to a maximum resolution of $(\sin\theta/\lambda)_{max} = 0.49$ Å^{-1} (Baron *et al.*, 1997) (see Table 2 for details).

[1] Supplementary material for this article is available from the IUCr electronic archive (Reference: WL5162). Services for accessing this material are described at the back of the journal.

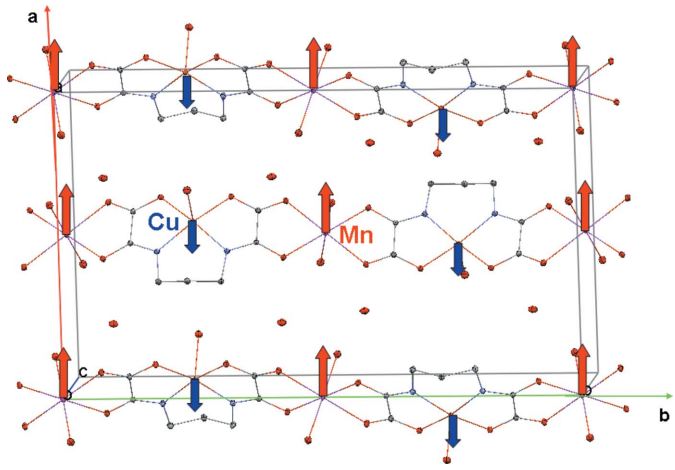

Figure 2
Crystal packing and spin magnetic moments of Mn and Cu aligned by an applied field along the crystallographic *a* axis (vertical).

To check the reliability of the joint refinement procedure, in the following we discuss in turn (i) the refinement of the charge density against the XRD data only (*MOLLY*), (ii) the refinement of the spin density against the PND data only (*MFLOP*; Boucherle *et al.*, 1982) and (iii) the joint refinement itself using the new software *MOLLYNX*. The first two studies will serve as benchmarks for the separated charge and spin densities prior to the joint XRD–PND treatment.

3.1. Benchmark charge-density refinement: XRD only

In order to model the total charge density at 10 K, a Hansen and Coppens multipolar refinement (Hansen & Coppens, 1978) was performed against the 6880 structure-factor amplitudes (F) with intensities $I > 3\sigma(I)$. The atomic positions and atomic displacement parameters of non-H atoms were first refined against high-order reflections ($\sin\theta/\lambda > 0.8$ Å^{-1}) to deconvolute the valence electron density from thermal smearing effects, leading to the best unbiased refined structural parameters. In this test case, UND data were not used. As a consequence, the atomic positions of H atoms may be biased. To circumvent this effect, the H atoms were displaced along their X—H bond to distances from tabulated values (Allen *et al.*, 1992). Then the valence- and symmetry-allowed multipolar parameters were refined until convergence with multipolar expansion (l) up to $l = 4$ for Cu, Mn, O and N atoms, and $l = 3$ for C atoms, while for all H atoms only the valence population and a dipole directed along the X—H bond were refined. Core and spherical valence charge densities were constructed using Clementi and Roetti Hartree–Fock wavefunctions (Clementi & Roetti, 1974), and the radial functions for the deformation density were single Slater-type functions with n_l and ζ_l as reported in Table 3.

A unique κ, κ' parameter set was used for each atomic type; κ'(H) was not refined. The final model with 422 parameters and 6880 reflections [$I > 3\sigma(I)$] led to $R(F) = 2.16\%$, $R_w(F) = 1.61\%$ and to a goodness of fit (GOF) of 1.58.

Table 3
The n_l and ζ_l parameters of Slater-type functions used in the multipolar refinement.

Atom type	n_l	ζ_l (bohr^{-1})
Cu	4, 4, 4, 4, 4	8.80
Mn	4, 4, 4, 4, 4	7.00
O	2, 2, 2, 3, 4	4.46
N	2, 2, 2, 3, 4	3.84
C	2, 2, 2, 3	3.18
H	1, 1	2.00

The featureless residual density map (Fig. 3*a*) attests to the XRD data quality and the relevance of the multipolar modelling. The static deformation density map (Fig. 3*b*) presents similar features to the 114 K data (Pillet *et al.*, 2004) with the main improvement being in the resolution of the lone-pair density of the O and N atoms due to the lower thermal smearing effect.

3.2. Benchmark spin-density refinement: PND only

In the previous study (Baron *et al.*, 1997) the spin-density refinement was performed against the experimental magnetic structure-factor amplitudes derived from the flipping ratios, which are the raw PND experimental quantities (Lecomte *et al.*, 2011). The published spin-density map was obtained using an $(x^2 - y^2)$ orbital constraint on the Cu atomic spin density, which slightly improved the agreement factors from a spherical refinement. In the *MOLLYNX* software, the model parameters are refined against the flipping ratios. In order to compare the quality of the results of the refinement using PND data alone with that obtained by joint refinement, a spherical-atom refinement was performed on the PND data only using *MFLOP* (Boucherle *et al.*, 1982). It led to the following agreement factors: $R(R)$ = 5.84%, $R_w(R)$ = 2.42% and a goodness of fit (GOF) of 1.93. The spin populations normalized to 2 μ_B per asymmetric unit are reported and compared to the joint refinement in Table 6. Note that the normalization is different to that applied by Baron and co-workers (Baron *et al.*, 1997), who set the sum of the spin populations of Mn, Cu and the bridging atoms equal to 4 μ_B. Different models were tested: the best fit was obtained when the spin density located on the Cu atom was restrained to arise from an $(x^2 - y^2)$-type orbital pointing toward the O and N atoms. This model improved the statistical agreement factor without changing the spin values on atoms with respect to their standard deviation, as shown by Baron *et al.* (1997) (Fig. 4).

3.3. Joint refinement strategy

The starting point of the joint refinement strategy was based on the charge- and spin-density multipolar models derived separately from the XRD and PND data, respectively, as discussed above. In order to have the best set of structural parameters, the atomic positions and X-ray atomic displacement parameters (x, y, z and U_{ij}^{X}) obtained from the previous multipolar refinement (XRD data only) were kept fixed and

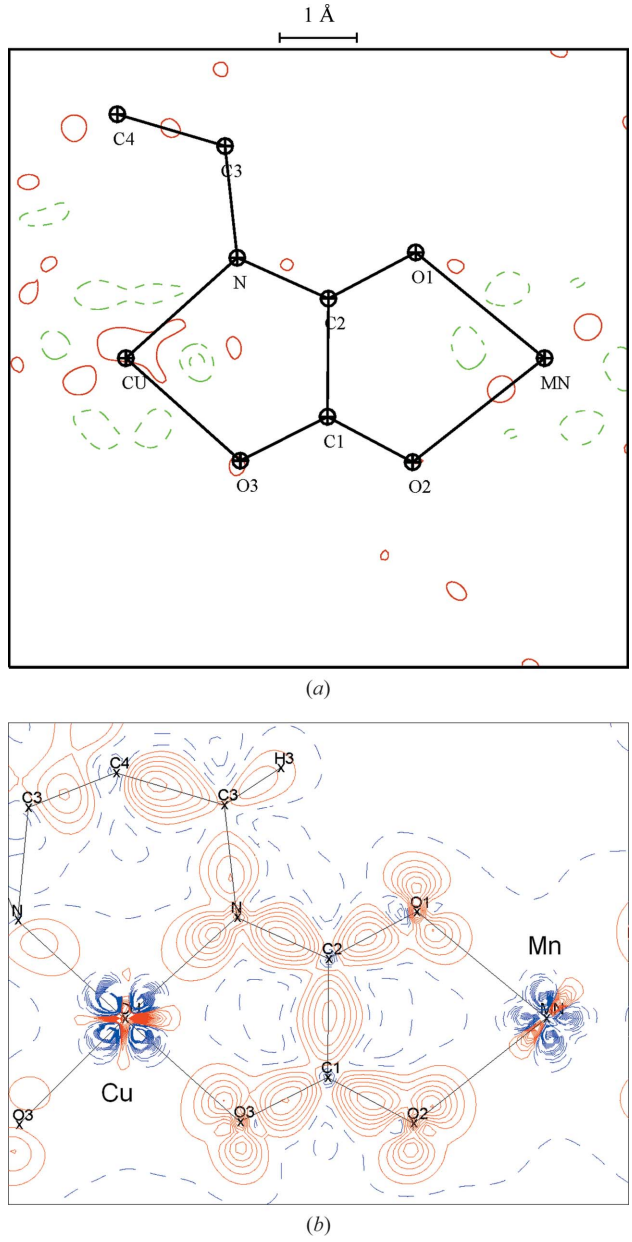

Figure 3
Charge density at 10 K. (*a*) Residual charge-density map (sin θ/λ < 0.8 Å^{-1}). (*b*) Static deformation charge-density map after the multipolar refinement (XRD data only) in the plane of the oxamato bridge. Contours are at intervals of 0.1 e Å^{-3}.

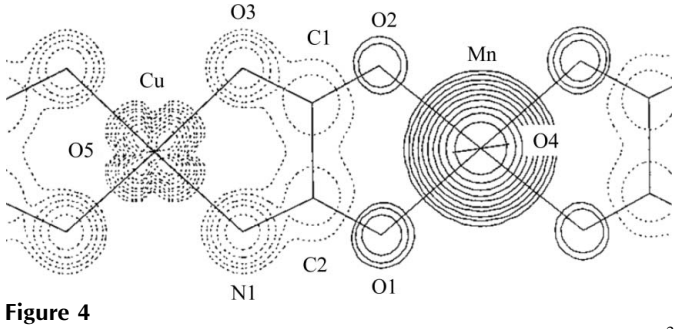

Figure 4
Projection of the spin density obtained from PND refinement with the $x^2 - y^2$ constraint from Baron *et al.* (1997). (Contours are at 0.005 × 2^{n-1} μ_B Å^{-2} with n = 1, 2, ...).

Table 4
Statistical agreement factors for P_v–κ refinement using different weighting schemes.

R^X (%)	$R_w{}^X$ (%)	GOF^X	R^{PN} (%)	$R_w{}^{PN}$ (%)	GOF^{PN}	Weight
2.91	2.87	2.73	8.25	2.98	2.38	UNIT
2.91	2.87	2.73	8.25	2.95	2.36	NLOG
2.91	2.88	2.74	7.55	2.87	2.29	LOG

the neutron atomic displacement parameters obtained in the previous study (Baron *et al.*, 1997) were not refined. Magnetic atoms (*i.e.* those expected to carry a significant spin magnetic moment) were defined according to the results of the benchmark spin-density results discussed above. They consist of the metallic atoms (Mn and Cu) and the atoms of the linking oxamato bridge (O1—O4, N, C1 and C2). For all those atoms, a split model [see equations (3) and (4)] was defined; their initial valence population parameters were set to half the values obtained in the benchmark XRD refinement. The Mn and Cu valence populations were introduced such that $\sum(P_v^{\uparrow} - P_v^{\downarrow})$ matches the number of unpaired electrons corresponding to the $S = 2$ state of the molecular unit formed by an Mn^{II} ion (s = 5/2) and a Cu^{II} ion (s = 1/2) that are antiferromagnetically coupled. This number is equal to 2 for the asymmetric unit, because Mn and Cu both lie on a symmetry element.

In the first step, it is important to assess what information can be extracted from both data sets with the joint refinement. For that purpose, a first refinement strategy was adopted as follows:

(1) The structural model of the benchmark XRD refinement was assumed, with the atomic displacement parameters of the benchmark XRD refinement kept fixed.

(2) Initially, all multipolar parameters $P_{lm\pm}$ were set to zero. (As a test case, to start with the least-biased model.)

(3) Then a P_v–κ joint refinement was performed (Coppens *et al.*, 1979).

(4) This was followed by a charge multipolar refinement against the XRD only.

(5) Finally, the joint charge- and spin-density multipolar refinement was performed.

The refinements were carried out using the three weighting schemes (UNIT, NLOG, LOG) and the three types of constraints between the multipolar parameters [unconstrained, *a posteriori* and cos(α) constraints].

In the following, the results of these refinements are compared in detail step by step.

3.3.1. P_v–κ joint refinement. In the first step, a P_v–κ joint refinement was conducted with all the multipolar parameters $P_{lm\pm}$ set to zero. The results are analyzed with respect to the refinement statistical agreement factors (given in Table 4) and the values of the refined parameters (given in Tables 5 and 6).

The refinement of the valence population, $P_v^{\uparrow}$ and $P_v^{\downarrow}$, using the three weighting schemes gave exactly the same statistical agreements and the same parameter values. The further refinement of κ slightly improved the statistical agreements for X-ray data while for PND it increased the agreement factors

Table 5
Values of the refined κ parameters for the different weighting schemes.
κ values for H atoms were not refined.

Atom	UNIT	NLOG	LOG	XRD data only (multipolar refinement)
Cu	1.021 (4)	1.020 (3)	1.019 (3)	1.002 (1)
Mn	1.032 (6)	1.027 (5)	1.003 (1)	1.010 (2)
O	0.976 (2)	0.975 (2)	0.973 (1)	0.976 (1)
N	0.988 (5)	0.987 (5)	0.990 (5)	0.979 (2)
C	1.048 (5)	1.047 (4)	1.045 (4)	1.006 (2)

for UNIT and NLOG weight; for the LOG weighting scheme they remain unchanged (Table 4).

With respect to their uncertainties, the κ values are statistically equal when using the three weighting schemes, except for Mn for which the κ value is slightly different with the LOG weighting scheme (Table 5). For example, for Mn, the difference is between 5 and 20σ. The refinement of $\kappa^{\uparrow}$ and $\kappa^{\downarrow}$ parameters for Cu and other atoms gave the same values within the standard deviation; it is noteworthy that for Mn splitting of the κ parameter was not possible since $P_v^{\downarrow}$ is almost zero, it was therefore decided in the further refinements not to split the κ parameters for all atoms; it also decreases the number of total parameters of the global model and avoids over-parameterization. This also makes it possible to achieve a better stability of the least-squares procedure by limiting the number of correlations.

The valence populations obtained after these refinements are summarized in Table 6; they are equal whatever the weighting schemes. Standard deviations are almost the same for UNIT and NLOG schemes but slightly smaller when using the LOG weighting scheme.

The spin-population values resulting from the joint refinement compare well with those of the refinement using only PND data. The resulting spin-density distribution shows spin up located on Mn and spin down on Cu, and a delocalization over the oxamato bridge, with positive spin contributions on the atoms in the neighbourhood of Mn and negative spin contributions on the Cu side, as already reported (Baron *et al.*, 1997). At this stage of the refinement it is therefore not possible to discriminate between the three weighting schemes.

These results also clearly show that the joint refinement is very robust and compares quite closely with the separate XRD-only and PND-only refinements.

3.3.2. Charge. After this joint refinement of the charge and spin valence populations, a multipolar refinement of the charge-density parameters (no $P_{lm\pm}$ splitting) was carried out and compared to the 'X-ray only' refinement. As expected, the agreement indices dropped significantly for the X-ray data set (R^X = 2.26% $R_w{}^X$ = 1.73%, GOF^X = 1.68, compared to 2.16%, 1.61% and 1.58 for the X-ray only refinement) without, of course, changing the PND indices. At this point of our test, the deformation density does not depend on the weighting scheme and is statistically equal to that refined against X-ray data only.

3.3.3. Spin-density multipolar refinement. At this stage of the joint refinement, all magnetic atoms exhibit a split valence

Table 6
Valence populations after P_v–κ joint refinement and comparison with the values obtained from the benchmark PND refinements.

	UNIT		NLOG		LOG		
Atom	$P_v^{\uparrow}, P_v^{\downarrow}$	$P_v^{\uparrow} - P_v^{\downarrow}$	$P_v^{\uparrow}, P_v^{\downarrow}$	$P_v^{\uparrow} - P_v^{\downarrow}$	$P_v^{\uparrow}, P_v^{\downarrow}$	$P_v^{\uparrow} - P_v^{\downarrow}$	PND data only
Cu	4.30 (2), 5.14 (2)	−0.84	4.30 (2), 5.14 (2)	−0.84	4.26 (2), 5.12 (2)	−0.86	−0.81 (3)
Mn	4.98 (4), 0.04 (2)	4.94	5.00 (4), 0.04 (2)	4.96	5.10 (2), 0.06 (2)	5.04	5.15 (4)
O1	3.25 (2), 3.23 (2)	0.02	3.25 (2), 3.23 (2)	0.02	3.25 (1), 3.23 (1)	0.02	0.02 (2)
O2	3.28 (2), 3.25 (2)	0.03	3.28 (2), 3.25 (2)	0.03	3.28 (1), 3.25 (1)	0.03	0.01 (1)
O3	3.21 (2), 3.23 (2)	−0.02	3.20 (2), 3.23 (2)	−0.03	3.20 (1), 3.23 (1)	−0.03	−0.05 (2)
O4	3.31 (2), 3.23 (2)	0.08	3.31 (2), 3.23 (2)	0.08	3.31 (1), 3.24 (1)	0.07	0.03 (1)
N	2.65 (3), 2.72 (3)	−0.07	2.65 (3), 2.72 (3)	−0.07	2.62 (3), 2.71 (3)	−0.09	−0.09 (2)
C1	1.76 (2), 1.78 (2)	−0.02	1.76 (2), 1.78 (2)	−0.02	1.75 (2), 1.78 (2)	−0.03	−0.05 (2)
C2	1.78 (2), 1.84 (2)	−0.06	1.78 (2), 1.84 (2)	−0.06	1.78 (2), 1.85 (2)	−0.07	−0.05 (2)

Table 7
Statistical agreement factors after spin-density multipolar refinement with the cos(α) constraints.

R^X (%)	$R_w{}^X$ (%)	GOF^X	R^{PN} (%)	$R_w{}^{PN}$ (%)	GOF^{PN}	Weighting scheme
2.18	1.63	1.55	7.37	2.34	1.97	UNIT
2.17	1.62	1.54	6.47	2.20	1.85	NLOG
2.19	1.65	1.57	6.42	2.11	1.77	LOG

Table 8
κ parameters after the spin-density multipolar refinement.

Atom		UNIT	NLOG	LOG	XRD data only (multipolar refinement)
Cu	κ	1.0156 (8)	1.003 (1)	1.0166 (8)	1.002 (1)
	κ'	1.03 (1)	1.04 (1)	1.02 (1)	1.04 (1)
Mn	κ	1.027 (2)	1.012 (2)	1.0222 (7)	1.010 (2)
	κ'	1.33 (3)	1.34 (3)	1.15 (2)	1.36 (3)
O	κ	0.9728 (5)	0.9751 (5)	0.9718 (5)	0.976 (1)
	κ'	0.98 (2)	0.95 (1)	0.80 (1)	0.96 (1)
N	κ	0.979 (2)	0.973 (2)	0.981 (2)	0.979 (2)
	κ'	0.89 (2)	0.84 (2)	0.84 (2)	0.87 (2)
C	κ	1.022 (2)	1.015 (2)	1.016 (2)	1.006 (2)
	κ'	0.96 (1)	0.90 (1)	0.96 (1)	0.87 (1)

population while their multipolar parameters are still not split. Therefore, the present model accounts for the asphericity of the charge density, but only for the isotropic contribution to the spin density through the split valence populations. This approximation may be released by splitting the multipolar parameters of magnetic atoms, starting from the previous charge-density multipolar refinement. For this purpose, it is necessary to define for which atom, and up to which multipole order, the refinement of the spin multipoles is relevant. The spin multipoles were split sequentially with increasing order, and the results were compared in order to ascertain the best refinement strategy. The joint refinements were performed using the cos(α) constraint, which is more rigorous. Symmetry-allowed multipolar parameters for Mn and Cu up to $l = 4$, only monopoles and dipoles for the other probable magnetic atoms, and κ and κ' were refined. The other atoms were refined following the standard manner (against XRD data only). This initial refinement was then followed by a splitting and refinement of all O, C and N quadrupoles, keeping the other parameters fixed (Figs. 5*b*–7*b*). The aim of this procedure was to decide whether there is some decisive non-spherical information in the PND data that can be retrieved from the joint fitting and then to refine the corresponding multipolar parameters in a second step.

These refinements were carried out for the three weighting schemes (UNIT, NLOG and LOG) until convergence. The corresponding statistical XRD agreement factors (Table 7) are close to those obtained for the refinement against XRD data only, while the best PND indices are, not surprisingly, obtained for the LOG weighting scheme ($R_w{}^{PN}$ = 2.11%) followed by the NLOG weighting scheme ($R_w{}^{PN}$ = 2.20%) and finally the UNIT weighting scheme ($R_w{}^{PN}$ = 2.34%).

The resulting density parameters are given in Tables 8 and 9, while the corresponding static deformation charge-density (Figs. 5*a*, 6*a* and 7*a*) and spin-density maps (Figs. 5*b*, 6*b* and 7*b*) are shown for the different weighting schemes.

Table 8 shows that the κ parameters are close whatever the weighting scheme. It is noteworthy that the refinement with the NLOG weighting scheme leads to results very close to the X-ray only refinement as expected: this weighting scheme favours mainly the X-ray data (§2.1). The deformation densities obtained in the UNIT and the NLOG refinement are very similar but slightly different to the LOG ones. The positive deformation density has a fourfold symmetry (Fig. 7*a*) on the Mn atom with lobes directed toward the ligand in the LOG case; it is very attenuated in the UNIT and the NLOG cases (Figs. 5*a* and 6*a*) with a small reduction (0.1 e Å^{-3}) in the lone-pair regions of O1, O2 and O3. This is due to the different Mn and O κ' values (Table 8: κ' varies from 1.34 to 1.15 and from 0.98 to 0.80, respectively). Several tests showed that this κ' variation for the O atoms was due only to a strong dipolar contribution on apical O4. The corresponding spin-density maps (Figs. 5*b*–7*b*) show a large dipole on O1 and a large quadrupolar contribution on O2 in the UNIT weight case, while in the LOG scheme there is no such large dipole and the quadrupolar contribution is similar on the two O atoms. O3 presents a dipole contribution in both cases. The C2 atom is always in a region of negative spin density while C1 is positive (UNIT) or slightly negative (LOG) depending on the weighting scheme.

Table 9 summarizes the spin populations obtained in the joint refinement compared to the previous study using PND data only. As expected, the Mn and Cu atoms carry large spin

Table 9
Spin population ($P_v^{\uparrow} - P_v^{\downarrow}$) after the spin-density multipolar refinement.

Atom	UNIT	NLOG	LOG	PND data only
Cu	−0.83 (3)	−0.84 (3)	−0.83 (2)	−0.81 (3)
Mn	5.05 (3)	5.13 (4)	5.14 (2)	5.15 (4)
O1	0.01 (2)	0.01 (3)	0.01 (2)	0.02 (2)
O2	0.01 (2)	0.01 (3)	0.02 (2)	0.01 (1)
O3	−0.04 (2)	−0.05 (3)	−0.07 (2)	−0.05 (2)
O4	0.05 (2)	0.04 (3)	0.03 (2)	0.03 (1)
N	−0.09 (3)	−0.12 (4)	−0.11 (2)	−0.09 (2)
C1	0.02 (3)	0.01 (4)	0.01 (3)	−0.05 (2)
C2	−0.07 (3)	−0.04 (4)	−0.03 (3)	−0.05 (2)

populations which do not depend on the refinement type. The main discrepancies are observed for C atoms, which carry the same moment in the PND refinements, while in the joint refinement C2 is always negative and C1 carries a small population ($\simeq$ the standard deviation), the sign of which depends on the constraints and the weighting scheme used. This underlines the fact that the standard deviations are a precise indication of the quality of the modelling.

3.4. Final 'most reasonable' joint refinement

From these refinements, it is hard to determine which spin multipoles must be refined for the ligand atoms, because all carry a small spin population with a small dipolar or quadrupolar contribution (close to their standard deviation), which can, however, change the shape of the spin distribution on these atoms. Despite the fact that the information in the PND data can in principle go up to octopolar level, like the charge density, the large correlation between multipolar parameters prevents this information from being extracting properly. Therefore, in this molecular crystal all the allowed multipoles up to $l = 4$ on metal atoms and monopoles only on the ligand atoms are relevant. This leads to what can be considered as the 'most reasonable' refinement. All the symmetry-allowed and split quadrupoles and hexadecapoles on Mn and Cu were refined because they are related to 3*d* orbital populations (Holladay *et al.*, 1983) and only split monopoles of the magnetic C, N and O atoms are refined. This approach is a good way to limit the number of refined parameters.

A flow chart of our proposed joint refinement procedure is presented in the supplementary material; however, we stress

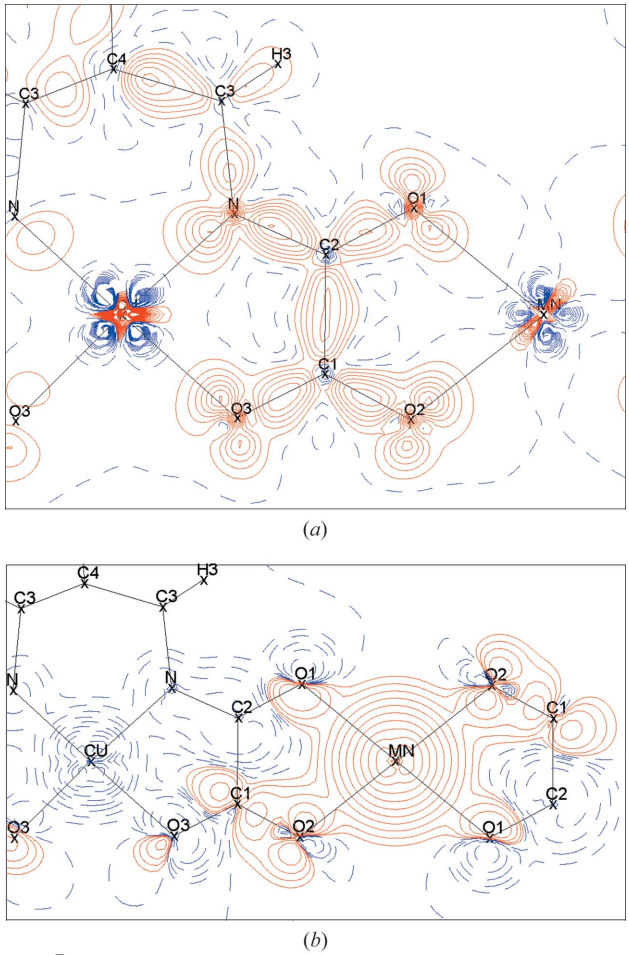

Figure 5
UNIT weighting scheme. (*a*) Static deformation charge-density map, contours as in Fig. 3. (*b*) Spin-density map with quadrupoles. Contours are at $\pm 0.01 \times 2^n\ \mu_B\ \text{Å}^{-3}$ ($n = 0, \ldots, 12$), positive: red lines, negative: blue dashed lines.

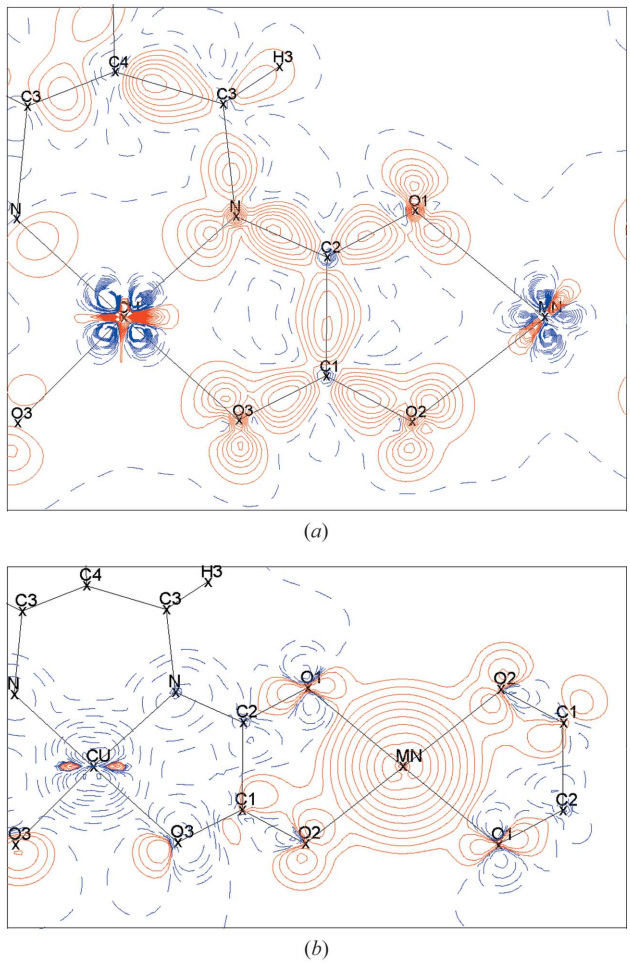

Figure 6
NLOG weighting scheme. (*a*) Static deformation charge-density map, contours as in Fig. 3. (*b*) Spin-density map with quadrupoles. Contours as in Fig. 5.

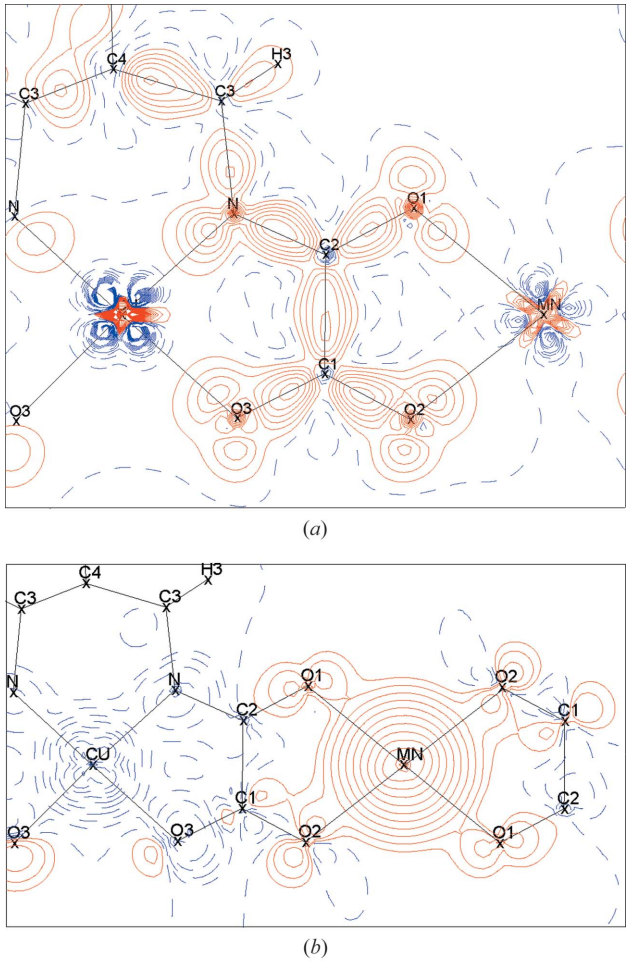

Figure 7
LOG weighting scheme. (*a*) Static deformation charge-density map, contours as in Fig. 3. (*b*) Spin-density map with quadrupoles. Contours as in Fig. 5.

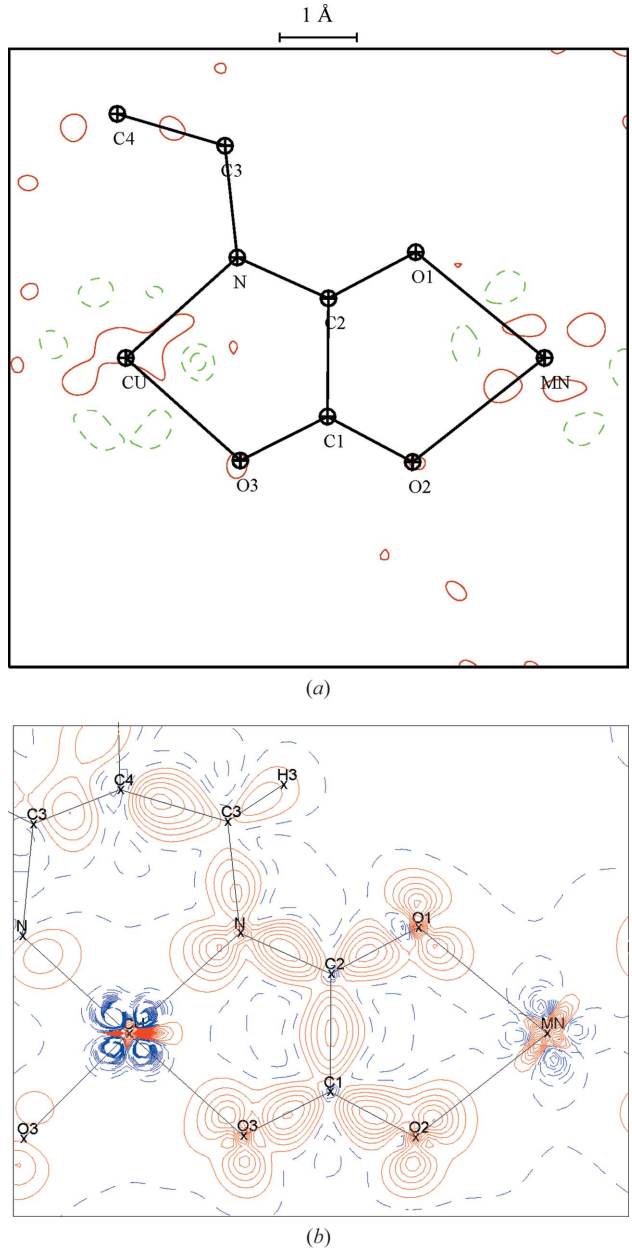

Figure 8
(*a*) Residual charge-density map (sin $\theta/\lambda < 0.8$ Å^{-1}); (*b*) static deformation charge-density map after the 'most reasonable' joint refinement using the LOG weighting scheme. Contours are at intervals of 0.1 e Å^{-3}.

that the joint refinement is at present NOT a routine procedure for obtaining the final parameters. Therefore, careful analysis of the results is of prime importance and the strategy of the procedure has to be adapted in each case. If after preliminary tests a parameter splitting turns out to be irrelevant, it is of course possible to return to the previous step and benefit from a simplification of the model.

This 'most reasonable' joint refinement (with the previous definition of 'reasonable') has to be compared with the refinement using XRD data only or PND data only (Figs. 8 and 9 *versus* Figs. 3 and 4, see also Table 10). The agreement factors are very similar: $R_w^X(F) = 1.63\%$ and $GOF^X = 1.58$, $R_w^{PN}(R) = 2.53\%$ and $GOF^{PN} = 2.17$.

The two distributions are very similar, but it has to be noted that a joint refinement has the advantage of not imposing any initial guess of the spin-density asphericity, as necessary for PND-only refinement (Baron *et al.*, 1997)

4. Conclusion

A joint refinement of charge and spin densities based on two different sets of XRD and PND data has for the first time been successfully carried out for a molecular magnetic compound. Owing to large correlations between the spin- and charge-density parameters, the application of constraints on the multipolar parameters is crucial for a stable, realistic joint refinement. Weighting schemes are of primary importance when dealing with experiments of different sizes and uncertainties. Despite a lack of rigorous mathematical foundation, the LOG weighting scheme appears to be the best compromise for combining XRD and PND data sets with different sizes. It allows the small number of PND data to be taken into account without any unreasonable influence on the XRD-based model.

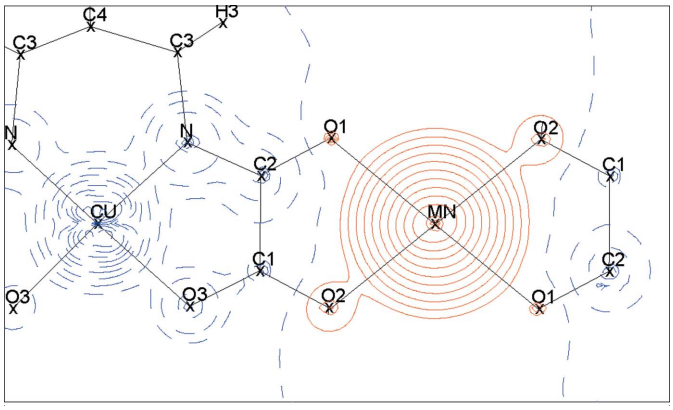

Figure 9
Spin density obtained by the 'most reasonable' joint refinement. Contours are at $\pm 0.01 \times 2^n\ \mu_B\ \text{Å}^{-3}$ ($n = 0, \ldots, 12$). Positive: red (Mn), negative: blue (Cu).

We have shown how the joint refinement strategy can be applied to data sets of different origins provided that one can construct a common description model. The proposed joint refinement procedure can obviously evolve when applied to other compounds. Studies involving the inclusion of other data such as Compton scattering are underway.

APPENDIX *A*
Calculation details for cos(*α*) constraint

The structure factors for X-ray and PND can be expressed as a function of $P^{\uparrow}_{lm\pm}$ and $P^{\downarrow}_{lm\pm}$ or P_{lmC} and P_{lmS} (the latter refer to the charge and spin multipolar populations, respectively):

$$F_{X,PN}(P^{\uparrow}_{lm}, P^{\downarrow}_{lm}, \ldots) = F'_{X,PN}(P_{lmC}, P_{lmS}, \ldots),$$

where $P_{lmC} = (P^{\uparrow}_{lm} + P^{\downarrow}_{lm})/2$ and $P_{lmS} = (P^{\uparrow}_{lm} - P^{\downarrow}_{lm})/2$. The derivatives of structure factors with respect to the charge and spin parameters are

$$\frac{\partial F'_{X,PN}(P_{lmC}, P_{lmS}, \ldots)}{\partial P_{lmC}} = \frac{\partial F_{X,PN}(P^{\uparrow}_{lm}, P^{\downarrow}_{lm}, \ldots)}{\partial P^{\uparrow}_{lm}} \frac{\partial P^{\uparrow}_{lm}}{\partial P_{lmC}} + \frac{\partial F_{X,PN}(P^{\uparrow}_{lm}, P^{\downarrow}_{lm}, \ldots)}{\partial P^{\downarrow}_{lm}} \frac{\partial P^{\downarrow}_{lm}}{\partial P_{lmC}}$$

and

$$\frac{\partial F'_{X,PN}(P_{lmC}, P_{lmS}, \ldots)}{\partial P_{lmS}} = \frac{\partial F_{X,PN}(P^{\uparrow}_{lm}, P^{\downarrow}_{lm}, \ldots)}{\partial P^{\uparrow}_{lm}} \frac{\partial P^{\uparrow}_{lm}}{\partial P_{lmS}} + \frac{\partial F_{X,PN}(P^{\uparrow}_{lm}, P^{\downarrow}_{lm}, \ldots)}{\partial P^{\downarrow}_{lm}} \frac{\partial P^{\downarrow}_{lm}}{\partial P_{lmS}}.$$

Using the cos(*α*) constraint [$P_{lmS} = \cos(\alpha) P_{lmC}$], the structure factors as function of P_{lmC} and cos(*α*) become

$$F''_{X,PN}(P_{lmC}\cos(\alpha), \ldots) = F'_{X,PN}(P_{lmC}, \cos(\alpha) P_{lmC}, \ldots).$$

The X-ray structure factors depend only on P_{lmC} while the PN ones depend on P_{lmC} and cos(*α*). Their derivatives are as follows.

Table 10
Spin populations of atoms after the 'most reasonable' joint refinement (LOG weighting).

Atom	$(P^{\uparrow}_{v} - P^{\downarrow}_{v})$	PND data only	$(P^{\uparrow}_{v} + P^{\downarrow}_{v})$	XRD data only
Cu	−0.85 (3)	−0.81 (3)	9.91 (3)	9.92 (4)
Mn	5.13 (2)	5.15 (4)	5.38 (2)	5.39 (4)
O1	0.01 (2)	0.02 (2)	6.39 (2)	6.40 (3)
O2	0.01 (2)	0.01 (1)	6.39 (2)	6.40 (3)
O3	−0.04 (2)	−0.05 (2)	6.37 (2)	6.38 (3)
O4	0.05 (2)	0.03 (1)	6.46 (2)	6.47 (3)
N	−0.10 (5)	−0.09 (2)	5.25 (5)	5.27 (6)
C1	−0.02 (4)	−0.05 (2)	3.85 (4)	3.83 (5)
C2	−0.05 (4)	−0.05 (2)	3.87 (4)	3.85 (5)

For XRD

$$\frac{\partial F''_X}{\partial P_{lmC}} = \frac{\partial F'_X}{\partial P_{lmC}} + \frac{\partial F'_X}{\partial P_{lmS}} \frac{\partial P_{lmS}}{\partial P_{lmC}} = \frac{\partial F'_X}{\partial P_{lmC}}$$

and the second derivative is null.

For PND

$$\frac{\partial F''_{PN}}{\partial P_{lmC}} = \frac{\partial F'_{PN}}{\partial P_{lmS}} \frac{\partial P_{lmS}}{\partial P_{lmC}} + \frac{\partial F'_{PN}}{\partial P_{lmC}} = \frac{\partial F'_{PN}}{\partial P_{lmS}} \cos(\alpha),$$

$$\frac{\partial F''_{PN}}{\partial P_{lm}} = \frac{\partial F'_{PN}}{\partial P_{lmS}} \frac{\partial P_{lmS}}{\partial \alpha_{lm}} = -\frac{\partial F'_{PN}}{\partial P_{lmS}} \sin(\alpha) P_{lmC}.$$

Second derivatives:

$$\frac{\partial^2 F''_{PN}}{\partial^2 P_{lmC}} = 0,$$

$$\frac{\partial^2 F''_{PN}}{\partial \alpha_{lm} \partial P_{lmC}} = -\frac{\partial F'_{PN}}{\partial P_{lmS}} \frac{\partial P_{lmS}}{\partial \alpha_{lm}} = -\frac{\partial F'_{PN}}{\partial P_{lmS}},$$

$$\frac{\partial^2 F''_{PN}}{\partial^2 \alpha_{lm}} = -\frac{\partial F'_{PN}}{\partial P_{lmS}} P_{lmC} \cos(\alpha).$$

These second derivatives were added to the inverse of the covariance matrices.

This work was supported by l'Agence Nationale de la Recherche (CEDA Project). MD thanks the CNRS for a PhD fellowship. The program *MOLLYNX* is available from MS on request.

References

Adams, P. D., Mustyakimov, M., Afonine, P. V. & Langan, P. (2009). *Acta Cryst.* D**65**, 567–573.
Allen, F. H., Kennard, O., Watson, D. G., Brammer, L., Orpen, A. G. & Taylor, R. (1992). *International Tables for Crystallography*, Vol. C, edited by A. J. C. Wilson, Table 9.5.1.1. Dordrecht: Kluwer Academic Publishers.
Baron, V., Gillon, B., Cousson, A., Mathonière, C., Kahn, O., Grand, A., Öhrström, L., Delley, B., Bonnet, M. & Boucherle, J.-X. (1997). *J. Am. Chem. Soc.* **119**, 3500–3506.
Becker, P. & Coppens, P. (1985). *Acta Cryst.* A**41**, 177–182.
Bell, B., Burke, J. & Schumitzky, A. (1996). *Comput. Stat. Data Anal.* **22**, 119–135.
Boucherle, J. X., Gillon, B., Maruani, J. & Schweizer, J. (1982). *J. Phys. Colloq.* C7, **43**, 227–234.

Brown, P. J., Capiomont, A., Gillon, B. & Schweizer, J. (1979). *J. Magn. Magn. Mater.* **14**, 289–294.
Claiser, N., Souhassou, M., Lecomte, C., Gillon, B., Carbonera, C., Caneschi, A., Dei, A., Gatteschi, D., Bencini, A., Pontillon, Y. & Lelièvre-Berna, E. (2005). *J. Phys. Chem. B*, **109**, 2723–2732.
Clementi, E. & Roetti, C. (1974). *At. Data Nucl. Data Tables*, **14**, 177–478.
Coppens, P., Boehme, R., Price, P. F. & Stevens, E. D. (1981). *Acta Cryst.* A**37**, 857–863.
Coppens, P., Guru Row, T. N., Leung, P., Stevens, E. D., Becker, P. J. & Yang, Y. W. (1979). *Acta Cryst.* A**35**, 63–72.
Coppens, P., Koritsanszky, T. & Becker, P. (1986). *Chem. Scr.* **26**, 463–467.
Coppens, P., Su, Z. & Becker, P. (1999). *International Tables for Crystallography*, Vol. C, edited by A. J. C. Wilson & E. Prince, ch. 8.7. Dordrecht: Kluwer Academic Publishers.
Duckworth, J. A. K., Willis, B. T. M. & Pawley, G. S. (1969). *Acta Cryst.* A**25**, 482–484.
Figgis, B., Kucharski, E. & Reynolds, P. (1989). *J. Am. Chem. Soc.* **111**, 1683–1692.
Gillet, J.-M. (2007). *Acta Cryst.* A**63**, 234–238.
Gillet, J.-M. & Becker, P. J. (2004). *J. Phys. Chem. Solids*, **65**, 2017–2023.
Gillet, J.-M., Becker, P. J. & Cortona, P. (2001). *Phys. Rev. B*, **63**, 235115.
Hamilton, W. C. (1965). *Acta Cryst.* **18**, 502–510.
Hansen, N. K. & Coppens, P. (1978). *Acta Cryst.* A**34**, 909–921.
Hirshfeld, F. L. (1977). *Isr. J. Chem.* **16**, 226–229.
Hohenberg, P. & Kohn, W. (1964). *Phys. Rev. B*, **136**, 864–871.
Holladay, A., Leung, P. & Coppens, P. (1983). *Acta Cryst.* A**39**, 377–387.
Howard, S., Huke, J., Mallinson, P. & Frampton, C. (1994). *Phys. Rev. B*, **49**, 7124–7136.
Jayatilaka, D. & Grimwood, D. J. (2001). *Acta Cryst.* A**57**, 76–86.
Koritsanszky, T. & Coppens, P. (1986). *Am. Crystallogr. Assoc. Annu. Rep.* **14**, p. 56.
Lecomte, C., Deutsch, M., Souhassou, M., Claiser, N., Pillet, S., Becker, P., Gillet, J.-M., Gillon, B. & Luneau, D. (2011). *Trans. Am. Crystallogr. Assoc.* http://www.amercrystalassn.org/documents/2011%20Transactions/Lecomte.pdf.
Massa, L., Goldberg, M., Frishberg, C., Boehme, R. F. & La Placa, S. J. (1985). *Phys. Rev. Lett.* **55**, 622–625.
Pei, Y., Verdaguer, M., Kahn, O., Sletten, J. & Renard, J. P. (1987). *Inorg. Chem.* **26**, 138–143.
Pillet, S., Souhassou, M. & Lecomte, C. (2004). *Acta Cryst.* A**60**, 455–464.
Ressouche, E., Boucherle, J.-X., Gillon, B., Rey, P. & Schweizer, J. (1993). *J. Am. Chem. Soc.* **115**, 3610–3617.
Stewart, R. F. (1976). *Acta Cryst.* A**32**, 565–574.
Williams, G., Figgis, B. & Mason, R. (1981). *J. Chem. Soc. Dalton Trans.* **3**, 734–742.
Williams, A., Kwei, G., Von Dreele, R., Raistrick, I. & Bish, D. (1988). *Phys. Rev. B*, **37**, 7960–7962.
Wlodawer, A. & Hendrickson, W. A. (1982). *Acta Cryst.* A**38**, 239–247.
Zheludev, A., Bonnet, M., Ressouche, E., Schweizer, J., Wan, M. & Wang, H. (1994). *J. Magn. Magn. Mater.* **135**, 147–160.